Interaction in the systems of fluid–melt–crystal

Chevychelov V.Yu., Korneeva A.A. Partitioning of Cl, H_2O and CO_2 in fluid-magmatic systems at $T = 1000°C$ and $P = 200$ MPa.

Institute of Experimental Mineralogy RAS, Chernogolovka Moscow district (chev@iem.ac.ru)

Abstract. The solubility of H_2O–CO_2–Cl-containing fluids of various concentrations (0, 3, 10, and 23 wt % of HCl and from 0 to ~8–15 wt % of CO_2) in dacite, phonolite, and rhyolite melts at 1000°C and 200 MPa was studied in experiments. It was shown that the Cl concentration in the melt increased substantially from rhyolite to phonolite and dacite (up to 0.25, 0.85, and 1.2 wt %, respectively). The introduction of CO_2 into the system resulted in an increase in the Cl content in the melt composition by 20–25%. One may suppose that Cl reactivity in a fluid increases in the presence of CO_2 to cause growth of the Cl content in the melt. The introduction of CO_2 into the system considerably affects the content of H_2O in aluminosilicate melts as well. Thus, the addition of CO_2 decreases the H_2O content in the melt by ~0.5–1.0 wt %. The decrease in the H_2O content in an aluminosilicate melt is probably caused by fluid dilution with CO_2 resulting in a decrease in the H_2O mole fraction and fugacity in the fluid.

Keywords: solubility, partitioning, experiment, aluminosilicate melkt, dacite, phonolite, rhyolite, fluid, volatile component, carbon dioxide, water, chlorine.

Volatile components (H_2O, CO_2, and Cl) are among the most characteristic in various magmatic processes. The separation of volatile matter from a magma melt is usually caused by a pressure fall and melt crystallization during the rising of magma from the deep Earth's crust, as well as by magma eruptions. The separation as such of volatile matter may be a motive force of the mentioned processes. Carbon dioxide and other carbon compounds, both raised with magma and formed from the assimilation of carbonate rocks by silicates, may have a considerable influence on the variation of the total solubility of other volatile components (e.g., of Cl) in magma (Dallai et al., 2011; Behrens et al., 2009). At present, the processes as such have been poorly studied.

Only a few publications are available on the influence of individual volatile components on the solubility of H_2O–Cl-containing fluid in magma melts. Thus, the addition of fluorine increases the chlorine content in a phonolite melt from 0.5 to 0.7 wt % at $T = 850°C$ and $P = 200$ MPa (Chevychelov et al., 2008). At the same time, the addition of sulfur at equal P–T conditions decreases the chlorine content in the rhyodacite melt from ~0.8 to ~0.7 wt % (Botcharnikov et al., 2004). The latter effect is caused by a decrease in the Fe content in the melt owing to binding with sulfur.

According to published data, dacite melts are characterized by higher CO_2 solubility owing to the presence of both molecular CO_2 and carbonate complexes compared to rhyolite or basalt melts of the prevailing molecular CO_2 or carbonate forms, respectively (Behrens et al., 2004a; 2004b; Botcharnikov et al., 2007). An increase in the water content in the melt composition results in a sufficient decrease in the molecular CO_2–carbonate ion ratio in the quenched glass (Botcharnikov et al., 2005).

Table 1. Compositions of the initial aluminosilicate melts (normalized for 100%)

Melt	SiO_2	TiO_2	Al_2O_3	FeO_{tot}	MgO	CaO	Na_2O	K_2O	A/CNK [a]
Dacite	66.7	0.8	16.7	4.1	1.4	3.6	4.0	2.7	1.05
Phonolite	57.5	-	21.8	2.2	0.2	3.0	5.7	9.6	0.87
Rhyolite	76.2	0.1	12.8	0.8	-	0.7	4.6	4.8	0.91
Andesite (Botcharnikov et al., 2007)	57.44	1.06	17.53	7.20	4.31	7.42	3.32	1.61	0.85

[a] A/CNK is the $Al_2O_3/(CaO + Na_2O + K_2O)$ mole ratio in the melt.

The authors have studied experimentally the solubility of H_2O–CO_2–Cl-containing fluids of different concentrations (0, 3, 10, and 23 wt % of HCl and from 0 to ~8–15 wt % of CO_2) in synthesized dacite, phonolite, and rhyolite melts (table 1) at $T = 1000°C$, $P = 200$ MPa, $\log f_{O_2}$ ~ (Ni–NiO) + 3.5, and an experiment duration of five days. Chlorine and CO_2 were added initially as HCl aqueous solutions and oxalic acid $H_2C_2O_4 \times 2H_2O$, respectively. About 5 mg of HCl solution, ~1.0–1.5 mg of oxalic acid, and ~50 mg of powdered previously synthesized aluminosilicate glass were placed into a platinum capsule. The experiments were carried out in internally heated high-pressure vessels.

After the experiment, the content of gaseous CO_2 in a capsule was determined by weight losses. The capsule was weighed, frozen in liquid nitrogen, punctured with a needle, and weighed anew after reaching room temperature. The amount of quenching aqueous chloride solution in the capsule was determined in a similar mode. The punctured capsule was weighed, then exposed for 3 min at 110°C, and weighed anew after cooling to room temperature. The glass composition and Cl content were determined using an EDX system and wave spectrometer combined with CamScan MV2300 electron microscope. No visible crystallization of aluminosilicate glass was detected. The water content in the glass was determined by Karl Fischer titration. The possible CO_2 content in the glasses was evaluated by published data (Behrens et al., 2009). One may suppose that the total CO_2 content was small (below 0.1 wt %). Since the experiments considered were carried out under conditions of water saturation, the water content in melts amounted to 4.5–6 wt %. The mole fractions of H_2O, CO_2, and Cl in fluids were calculated in view of the mass balances. The procedure of experiments as such, along with the conditions of analyzing the obtained quenching phases, is described in more detail in (Chevychelov et al., 2008).

The data obtained in the experiments on H_2O–CO_2–Cl fluids were compared to those of similar experiments on H_2O–Cl fluids and to published data for the andesite melt (Botcharnikov et al., 2007) (table 1; Fig. 1).

It is shown that the Cl content in the melt increases considerably from the rhyolite, phonolite, dacite, and andesite compositions (up to 0.25, 0.85, 1.2, and 2.8 wt %), which is primarily caused by growth of the concentration of Ca and, probably, of Mg and Fe in the melt composition. The authors found previously that the growth in the concentration of bivalent alkaline-earth elements (especially of Ca) in the melt composition caused the greatest increase in the Cl content in the melt (Chevychelov, Suk, 2003). A likely mechanism of Cl introduction into the structure of the granodiorite melt was proposed (Chevychelov et al., 2003).

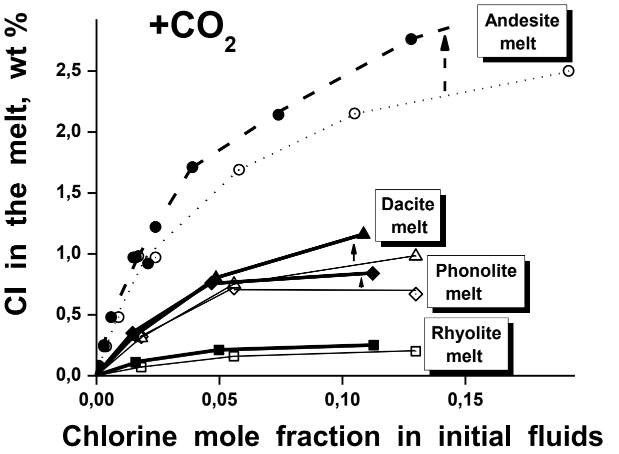

Fig. 1. The influence of CO_2 and the melt composition on the chlorine content in the melt. The authors' data for dacite, phonolite, and rhyolite compositions; the andesite melt by (Botcharnikov et al., 2007). See Fig. 2 for signs of different melt and fluid compositions. The thick and thin lines show the experiments on CO_2–H_2O–Cl- and H_2O–Cl-fluids, respectively.

The addition of CO_2 to the system results in an increase in the Cl content in all the melts treated (Fig. 1). With small amounts of Cl in the experiments, CO_2 increases the Cl content in the melt by 5–10%. This growth is enhanced by the increase in the total Cl content in the fluid. Thus, at a Cl mole fraction in the fluid over 0.10, the Cl concentrations in the melt increase in the CO_2-containing system by even 20–25% relative to the data of experiments without CO_2. One may assume that the presence of CO_2 increases the Cl reactivity in the fluid to cause a growth in the Cl content in the melt.

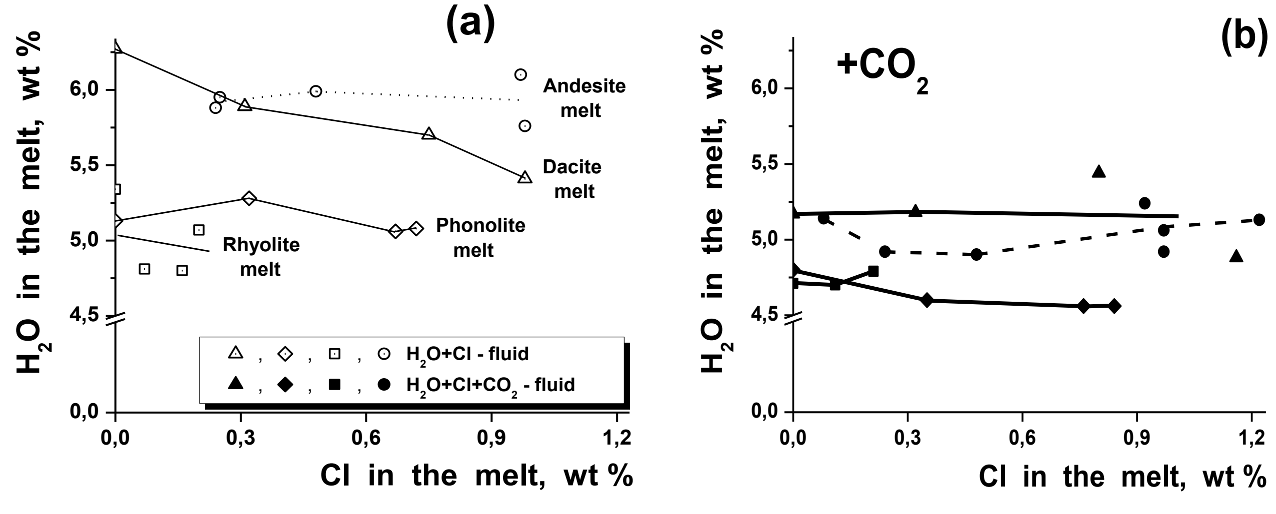

Fig. 2. The influence of CO_2 and the melt composition on the H_2O content in the melt. (a) Experiments on H_2O–Cl-fluids and (b) experiments on CO_2–H_2O–Cl-fluids. See Fig. 1 for other notations.

The introduction of CO_2 into the system affects the H_2O content in aluminosilicate melts as well (Fig. 2). Thus, the addition of CO_2 decreases the H_2O content in the melt by ~0.5–1.0 wt %. The decrease in the H_2O content in the aluminosilicate melt under the addition of CO_2 is probably caused by fluid dilution with carbon dioxide resulting in a decrease in the H_2O mole fraction and fugacity in a fluid.
One must note that CO_2 solubility in the phases of a system and, quite possibly, the effect of CO_2 on the behavior of other volatile components might be considerably modified, probably towards the growth, in the case of a lower H_2O content in the system and in the melts undersaturated with aqueous fluid.

Acknowledgments. This study was supported by the Russian Foundation for Basic Research (project No 15-05-03393-a) and by the program Integrated Studies on Topical Problems of Earth Sciences of the Branch of Earth Sciences, Russian Academy of Sciences.

References:

1. *Chevychelov V.Yu., Simakin A.G., Bondarenko G.V.* Mechanism of Chlorine Dissolution in Water-Saturated Model Granodiorite Melt: Applications of IR Spectroscopic Methods // Geochemistry International. 2003. Vol. 41. № 4. P. 395-409.
2. *Chevychelov V.Yu., Suk N.I.* Influence of the Composition of Magmatic Melt on the Solubility of Metal Chlorides at Pressures of 0.1–3.0 kbar // Petrology. 2003. Vol. 11. № 1. P. 62-74.
3. *Behrens H., Misiti V., Freda C., Vetere F., Botcharnikov R.E., Scarlato P.* Solubility of H_2O and CO_2 in ultrapotassic melts at 1200 and 1250°C and pressure from 50 to 500 MPa // American Mineralogist. 2009. V. 94. P. 105-120.
4. *Behrens H., Ohlhorst S., Holtz F., Champenois M.* CO_2 solubility in dacitic melts equilibrated with H_2O-CO_2 fluids: Implications for modeling the solubility of CO_2 in silicic melts // Geochimica et Cosmochimica Acta. 2004a. V. 68. No 22. P. 4687-4703.
5. *Behrens H., Tamic N., Holtz F.* Determination of the molar absorption coefficient for the infrared absorption band of CO_2 in rhyolitic glasses // American Mineralogist. 2004b. V. 89. P. 301-306.
6. *Botcharnikov R.E., Behrens H., Holtz F., Koepke J., Sato H.* Sulfur and chlorine solubility in Mt. Unzen rhyodacitic melt at 850°C and 200 MPa // Chemical Geology. 2004. V. 213. No 1-3. P. 207-225.
7. *Botcharnikov R., Freise M., Holtz F., Behrens H.* Solubility of C-O-H mixtures in natural melts: new experimental data and application range of recent models // Annals of Geophysics. 2005. V. 48. No 4/5. P. 633-646.
8. *Botcharnikov R.E., Holtz F., Behrens H.* The effect of CO_2 on the solubility of H_2O-Cl fluids in andesitic melt // Eur. J. Mineral. 2007. V. 19. P. 671-680.
9. *Chevychelov V.Yu., Botcharnikov R.E., Holtz F.* Partitioning of Cl and F between fluid and hydrous phonolitic melt of Mt. Vesuvius at ~850-1000°C and 200 MPa // Chemical Geology. 2008. V. 256. No 3-4. P. 172-184.
10. *Dallai L., Cioni R., Boschi C., D'Oriano C.* Carbonate-derived CO_2 purging magma at depth: Influence on the eruptive activity of Somma-Vesuvius, Italy // Earth and Planetary Science Letters. 2011. V. 310. No 1-2. P. 84-95.

Chevychelov V.Yu. Partitioning of Pb and Zn in the process of granite melt crystallization at pressure near 270 and 510 mPa.

Institute of Experimental Mineralogy RAS, Chernogolovka Moscow district (chev@iem.ac.ru)

Abstract. During the preparation of the experiments sample of water-saturated glass contained PbO and ZnO was placed in Pt capsule and sealed. Crystallization was carried out by slow decrease of temperature at two pressures (*P* ~270 and ~510 MPa): *T* = 630 → 580°C, *P* = 285 → 255 MPa and *T* = 600 → 550°C, *P* = 520 → 500 MPa. The solid phases, crystallizing in the system, are represented by quartz and feldspars: albite (*Ab*), oligoclase (*Olg*), anorthoclase (*Ancl*) and K_2O enriched feldspar (*Kfs*). A significant influence of pressure on the partitioning of polymetals between the fluid, evolved from the granite melt, and crystallizing feldspars has been established. Thus, at *P* ~ 270 MPa, zinc is preferentially concentrated in the fluid than in the crystalline phases. Lead enters uniformly into different phases. At *P* ~ 510 MPa the contents of polymetals in the fluid decrease by more than an order of magnitude, while the lead content in *Olg* and *Kfs* increases significantly (by a factor of 6-7). At this pressure the lead begin to concentrate mainly in feldspars.

Keywords: solubility, partitioning, experiment, crystallization, granite melt, fluid, minerals, feldspar, albite, oligoclase, anorthoclase, potassic feldspar, lead, zinc.

During the crystallization of the granite melt the components are distributed between three or more phases: the evolved fluid, the formed crystalline phases (several) and the residual melt. At an experimental study of this phenomenon we encountered serious difficulties due to the fact that at a temperature above the solidus crystallization of the granite melt proceeds extremely slowly, owing to the high viscosity of the melt. Therefore the experiments were carried out in the subsolidus region, but near solidus at a pressure of at least 250 MPa. At these conditions we obtained a sufficiently high degree of crystallization of the granitic melt (more than 50 vol.%), and the fluid evolved during crystallization was close to equilibrium with crystalline phases and residual melt.

During the preparation of the experiments a sample of water-saturated glass (~1 g), pre-melted from Akchatau massif granite and contained ~0.4-0.5 wt % PbO and as many ZnO, was placed in Pt capsule and sealed. Crystallization was carried out by slow decrease of temperature at two pressures (*P*

~270 and ~510 MPa): $T = 630 \rightarrow 580^{o}C$, $P = 285 \rightarrow 255$ MPa and $T = 600 \rightarrow 550^{o}C$, $P = 520 \rightarrow 500$ MPa. The experiments were carried out by an exoclave hydrothermal apparatus at a f_{O2} close to the Ni-NiO buffer pair. To extract the fluid, that formed during crystallization, from the intercrystalline pores an isochoric quenching was used, at which with decreasing temperature the pressure was dropped at such rate that the maximum permissible free volume of the capsule was maintained. After the experiment the bulk of the solution was in the sample-free part of the capsule and was easily retrieved under the action of internal pressure at cautious pricking the capsule wall by a thin needle.

After the experiment the formation of large cavities in the central part of the quenching samples was observed, the walls of which were composed of sufficiently large crystals of feldspars and quartz, up to 50-100 μm in size. The chemical composition of crystalline phases and quenching glass was determined using a microprobe analysis in two stages: first the total phase composition was determined by an energy-dispersive spectrometer, and then the contents of Pb and Zn were more precisely determined at the same point (probe size about 5 μm) by a wave dispersion spectrometer. The solid phases, crystallizing in the system, are represented by quartz and feldspars: albite (*Ab*), oligoclase (*Olg*), anorthoclase (*Ancl*) and K_2O enriched feldspar (*Kfs*) of uncertain species. In quartz the impurities of lead and zinc are not detected.

In the residual melt the contents of polymetals decrease to 0.2-0.3 wt % PbO and ZnO. The pH of quenching solutions was ~ 4.0 at *P* ~ 270 MPa and ~ 6.0 at *P* ~ 510 MPa. These values are in good agreement with the previously revealed pattern of decrease in the acidity of the fluid with increasing pressure (Chevychelov, Chevychelova, 1997). The fields of the melt (glass), remaining after crystallization, have rather large sizes from 50 to 1000 and more microns. Despite some heterogeneity of these residual melts with respect to the contents of K, Na, Ca, and partly Fe and Al, the concentrations of polymetals in them are fairly constant (about 0.2-0.3 wt %). These concentrations are twice lower than in the initial (0.4-0.5 wt% PbO and ZnO) melt. Only a few residual melt compositions are an exception, in which an increase in the PbO content correlates with an increase in CaO.

Table 1 shows the contents of Pb and Zn in the fluid, feldspars, as well as the partition coefficients of polymetals between these phases. Probably it is more correct to call them "effective" partition coefficients, since they are calculated from data obtained from nonequilibrium experiments.

Table 1. Lead and zinc concentrations in crystallized feldspars and in fluid evolved from the melt, and the "effective" partition coefficients of the polymetals (at initial 0.1*N* HCl + 1*N* NaCl solution and ~12-13 days run duration)

	$T = 630 \rightarrow 580^{o}C$, $P = 285 \rightarrow 255$ MPa		$T = 600 \rightarrow 550^{o}C$, $P = 520 \rightarrow 500$ MPa	
	Pb	Zn	Pb	Zn
$^{fluid}C$, wt %	0.27±0.07	0.23±0.05	0.02±0.01	0.016±0.005
^{Ab}C, wt %	0.25	0.04	0.4	< 0.015
^{Olg}C, wt %	-	-	1.76	0.24
^{Ancl}C, wt %	0.28	0.03	-	-
^{Kfs}C, wt %	0.3	0.24	1.76	0.08
$^{fluid/Ab}D$	1.1	6	0.05	> 1.1
$^{fluid/Olg}D$	-	-	0.01	0.07
$^{fluid/Ancl}D$	1	8	-	-
$^{fluid/Kfs}D$	0.9	1	0.01	0.2

A significant influence of pressure on the partitioning of polymetals between the fluid, evolved from granite melt, and crystallizing feldspars has been established. Thus at *P* ~ 270 MPa zinc is preferentially concentrated in the fluid than in the crystalline phases, with the exception of *Kfs*; and lead uniformly enters into different phases, since the lead partition coefficients are close to unity. At *P* ~ 510 MPa the content of polymetals in the fluid decreases by more than an order of magnitude, concurrently the lead content in *Olg* and *Kfs* increases significantly (by a factor of 6-7). At this pressure the polymetals begin to concentrate mainly in feldspars (with the exception of Zn in *Ab*), and to a greater extent in *Olg* and *Kfs*. We can note a negative correlation between the contents of PbO (ZnO) and SiO_2 in the composition of feldspars, which probably reflects a change in the content of the anorthite component.

Lead-containing feldspar of the $PbAl_2Si_2O_8$ composition (analog of anorthite), in which lead completely replaces calcium, was synthesized by the

authors of the publications (Scheel, 1971, Bruno, Facchinelli, 1972, Bambauer et al., 1974) by several ways. For example, there were from a mixture of oxides in platinum crucibles at T = 1150°C, P = 0.1 MPa and the 12 hours run duration, as well as by hydrothermal synthesis from a gel at T = 520°C, P_{H2O} = 120 MPa, and the 120 hours run duration. Taroev et al. (1990, 1997) experimentally showed that the occurrence of Pb in potassium feldspar is very limited and does not exceed 0.33 (0.5) wt % PbO at hydrothermal oxidative conditions (Cu-Cu_2O buffer pair) at T up to ~ 500°C and P = 100 MPa, and at reductive conditions (Ni-NiO buffer pair) PbO content is <0.05 wt %. Although it is known that at natural conditions the highest concentrations of Pb (up to 1-2 wt %) are characteristic of amazonites (*Kfs*). The partition coefficient of Pb ($^{fl/Kfs}D_{Pb}$) is also estimated in (Taroev et al., 1997), which at oxidative conditions (Cu-Cu_2O buffer pair) is ~ 1.25 ± 0.3.
At the same time we are not aware, and the summary (Bambauer et al., 1974) does not given experimental or natural data on the limits of the occurrence of zinc in feldspars. Although it can be assumed that zinc also replaces calcium in the structure of feldspars. The obtained results make it possible to estimate the limits of this occurrence. At our studied conditions at P ~ 500 MPa the feldspars (*Olg*) can contain up to ~ 0.5 wt% ZnO.

Apparently in our experiments the lead may be present in the structure of feldspars in the form of "lead anorthite" complex-minal ($PbAl_2Si_2O_8$), or by replacing two potassium atoms with the formation of one cation vacancy in *Kfs* ($PbAl_2Si_6O_{16}$). Zinc at these conditions is likely to remain in the melt or in *Olg*, marginally entering in *Ab*. The experimentally obtained content of Zn in *Ab* is the lowest among the feldspars; it is in good agreement with natural geochemical data (Antipin et al., 1984). It can be assumed that the Zn deficiency by mass balance is related to the formation of its own minerals such as franklinite (Zn,Fe,Mn)$(Fe,Mn)_2O_4$ or zincite (Zn,Mn)O. Natural geochemical data indicate that during the crystallization of acid magmatic rocks the feldspars concentrate Pb better than other minerals. While Zn is mainly accumulated in mica and amphiboles, replacing bivalent magnesium and iron (Antipin et al., 1984).

Figure 1 shows the effect of pressure on the partitioning of polymetals. Attention is drawn to the noticeable difference in the behavior of Pb and Zn in this system. With decreasing pressure the partition coefficients of Pb and Zn increase, but to different degrees: for Pb it is 1.5-2 orders of magnitude, and for Zn it is ~ 5 times. If in the fluid the concentrations of these elements are close to each other, then the feldspars may contain much more Pb than Zn. This increase in Pb is due to an increase in the "anorthite component" content and an increase in pressure. Thus at ~ 510 MPa the Pb content in feldspars is 1-2 orders of magnitude greater than in the fluid; and the Zn content in *Ab* is close to its content in the fluid and essentially increases only in *Olg* and *Kfs*, although it is to a lesser extent than for Pb.

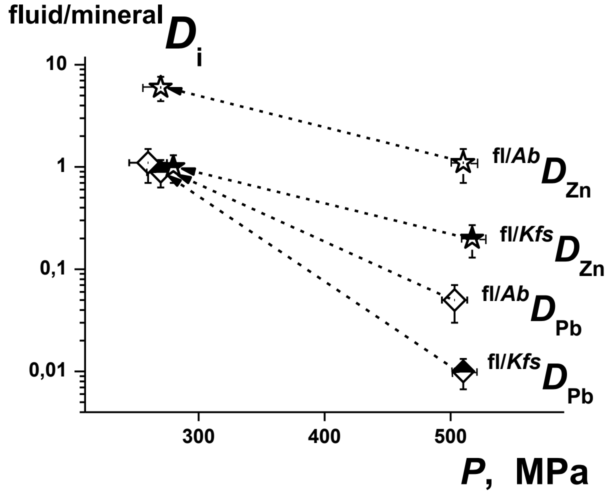

Fig. 1. The effect of pressure on the "effective" partition coefficients of Pb and Zn between the evolved fluid and feldspars crystallized from the melt**.**

It can be assumed that the crystallization of granite massifs at different depths will produce a magmatogenic fluid with different degrees of potential ore bearing, if other conditions being equal. A greater potential productivity with respect to polymetals (Pb, Zn) will have the less deep-seated magmatic bodies (~ 250 MPa). At the conditions of more deep magmatic crystallization (~ 500 MPa), in the zone of magma generation, the lead will practically not fractionate into the fluid, concentrating in *Pl* and *Kfs*, which, as a result of further interaction with the fluids and recrystallization, can become the source of ore material at the postmagmatic stage. Zinc, unlike lead, is much less accumulating in feldspar. And since these metals occur together in ore deposits, the formation of ore-bearing fluids associated with leucocratic granites by the mechanism of solid → fluid at the postmagmatic stage seems less preferable compared to the formation of high-temperature ore-bearing magmatic fluid as a result of the interaction melt → fluid, at which the behavior of Pb and Zn is more similar.

Acknowledgments. This study was supported by the Russian Foundation for Basic Research (project No 15-05-03393-a) and by the program Integrated Studies on Topical Problems of Earth Sciences of the Branch of Earth Sciences, Russian Academy of Sciences.

References:

1. *Antipin V.S., Kovalenko V.I., Ryabchikov I.D* Rare element partition coefficients in magmatic rocks. M.: Nauka, 1984. 254p. (in Russian).

2. *Taroev V.K., Tauson V.L., Piskunova L.F., Abramovich M.G.* Preparation of potassium feldspar crystals and study of the accumulation of lead in FSP in hydrothermal conditions // Geologiya I Geophyzika. 1990. № 2. P.66-75. (in Russian).
3. *Taroev V.K., Tauson V.L., Suvorova L.F., Pastushkova T.M., Proidakova O.A., Barankevich V.G.* Partitioning of lead between potassium feldspar and fluid of alkaline composition in the SiO_2-Al_2O_3-PbO_2-KOH-H_2O system at temperature of 500°C and pressure of 100 MPa // Doklady Akademii Nauk. 1997. V. 357. № 6. P.815-817. (in Russian).
4. *Bambauer H.U., Kroll H., Nager H.E., Pentinghaus H.* Feldspat-Mischkristalle - eine Ubersicht // Bull. Soc. fr. Mineral. Cristallogr. 1974. V. 97. P.313-345.
5. *Bruno E., Facchinelli A.* Al, Si configurations in lead feldspar // Ztschr. Kristallogr. 1972. Bd. 136. S.296-304.
6. *Chevychelov V.Yu., Chevychelova T.K.* Partitioning of Pb, Zn, W, Mo, Cl and major elements between aqueous fluid and melt in the systems granodiorite (granite, leucogranite) – H_2O – NaCl – HCl // N. Jb. Miner. Abh. 1997. V. 172. No 1. P.101-115.
7. *Scheel H.J.* Lead feldspar // Ztschr. Kristallogr. 1971. Bd. 133. S.264-272.

Lipko S.V.[1], Tauson V.L.[1], Balakleyskiy N.S.[2], Shermetova M.A.[2], Loginov B.A.[2] Surficial non-autonomous phase formation conditions and their effect on distribution of Pt and Pd in multi-component hydrothermal systems.

[1]A.P.Vinogradov Institute of Geochemistry SB RAS, Irkutsk (LIPKO@IGC.IRK.RU), [2]National Research Institute MIET, Zelenograd, Moscow

Abstract. The surficial non-autonomous phases (SNAPs) are formed more probably in the multi-component systems. The crystals of bornite, galena, magnetite, pyrite and chalcopyrite were synthesized in multi-phase associations in the system ZnS-PbS-Cu_2S-Fe-S with Pt and Pd micro-admixtures under hydrothermal conditions. The surface of crystals obtained was studied by the methods of X-ray diffraction (XRD), atomic force microscopy (AFM), scanning tunneling microscopy (STM) and X-ray photoelectron spectroscopy (XPS). The SNAP morphological parameters and superficially bound trace elements are studied. SNAP morphology is shown to be dependent on the concentration of mineralizer in solution. XPS showed two forms of Pt and Pd presence being the elemental and oxidized ones. The trace element contents are mainly dependent on the possibility of their inclusion into SNAP.

Keywords: non-autonomous phase, multi-component system, magnetite, hydrothermal crystal growth, Pt, Pd, AFM, STM, XPS

Introduction. It was previously shown that surficial non-autonomous phases (SNAP) play an active role both in crystal growth and the process of distribution of trace elements in the host mineral systems (Tauson et al., 2014). In turn, the structural characteristics, composition and properties of SNAP are largely determined by the environment, since these phases, in a sense, are transitional between ambient solution and the crystalline phase volume. It was also found that the pyrrhotite-like SNAP is formed on pyrite; its composition is $Fe^{2+}[S, S_2, S_n]^{2-}$ and it is capable of concentrating anionic (SO_3^{2-}, SO_4^{2-}, $S_2O_3^{2-}$) and cationic admixtures including precious metals. SNAP on magnetite is represented by oxyhydroxide phase, similar to hydromagnetite (Tauson et al., 2016), on galena-by sulphoxychloride phase (Tauson et al., 2005). Morphological characteristics and chemical composition of SNAP depend on the fugacities of oxygen and sulfur in the system, its complexity and other factors. The present paper presents the study of SNAP forming on crystals of minerals growing in complex multiphase systems at different concentrations of the solvent. The role of SNAP in concentrating of precious metals is demonstrated.

Experiment and analysis methods. We used the traditional technique of hydrothermal thermogradient synthesis at 450°C and pressure 1 kb with a 15 – degree temperature drop on the external wall of the autoclave. Ammonium chloride based solutions were used. 1% of each of the noble metals (Pt, Pd) were added to the system of ZnS-PbS-Cu_2S-Fe-S, with the view to study their distribution on the surface of obtained crystals upon completion of the experiment. Compositions of the original load and solution as well as phases obtained in the experiments are listed in Table 1. Mineral composition of the products was determined by X-ray analysis.

The crystals obtained were analyzed by the following methods and devices. X-ray diffraction analysis (XRD) was performed by powder method on the diffractometer D8 ADVANCE manufactured by "BRUKER". Microscopic analysis of the surface was carried out on scanning probe microscope SMM-2000 manufactured in Russia (factory PROTON, Zelenograd). Galena crystals were studied by atomic force microscopy (AFM), using silicon nitride cantilever probes manufactured by Veeco (USA) with probe curvature radius of 10 nm and with the maximum controlled resolution in the XY plane about 2.5 nm, in the Z direction – approximately 1 nm. Magnetite crystals were also studied by higher resolution method of scanning tunneling microscopy (STM) with the use of platinum needle–shaped probes; maximum controlled resolution in the XY plane reached about 0.5 nm, in the Z direction - about 0.2 nm. Chemical state of precious metals in the surface was defined by the method of X-ray photoelectron spectroscopy (XPS) on the LAS-3000 unit manufactured by "Riber" (France).

Table 1. Experimental conditions and the phases acquired in crystal-synthesis experiments in the system of ZnS-PbS-Cu_2S-Fe-S (+ Pt, Pd)-NH_4Cl-H_2O at 450°C and at pressure of 1 kb

	Initial batch composition, wt.%					Solution composition	Phases obtained*
	ZnS	PbS	Cu_2S	Fe	S		
1	30	30	20	20	-	5%NH_4Cl	Bor, Mt, Sph, Gn
2	30	30	20	20	-	10%NH_4Cl	Mt, Sph, Bor, Cpy,Gn
3	30	30	20	20	-	10%NH_4Cl+ 2%$K_2Cr_2O_7$	Sph, Mt, Gn
4	30	30	10	15	15	5%NH_4Cl	Py, Cpy, Sph, Gn, Mt
5	30	30	10	15	15	10%NH_4Cl	Py, Sph, Gn, Bor
6	30	30	10	15	15	10%NH_4Cl+ 2%$K_2Cr_2O_7$	Gn, Sph

* Bor – bornite, Cu_5FeS_4; Mt – magnetite, Fe_3O_4; Sph – sphalerite (Zn, Fe)S; Gn-galena, PbS; Cpy-chalcopyrite, $CuFeS_2$; Py-pyrite, FeS_2.

Experiment results and discussion. The sulphide and magnetite crystals obtained did not normally exceed 2 mm in diameter, with no significant differences observed in the size of crystals. Galena (Fig. 1) and magnetite (Fig. 2) crystals show that increase in the mineralizer concentration from 5 to 10% induces SNAP structure ordering. The main parameters that characterize surface morphology of the surface also markedly change (Table 2). These data argue for SNAP formation during growth process controlled by oversaturation, which differs for 5 and 10% solution. However, the proximity of the crystal sizes in the experiments presumes that this effect is not kinetic in nature. That is, it is related not to the growth rate, but to the change in composition and structure of the SNAP participating in the crystal growth process. During crystallization, not the volume of crystal, but its surface layer attains equilibrium with the solution. This layer is structurally reconstructed and chemically modified into SNAP, inseparable from matrix crystal. Altered state of the layer is accounted for by the fact that the solid phase in equilibrium with the oversaturated solution is characterized by a higher chemical potential as compared to solid phase in a saturated solution. An excess of chemical potential can show both in the change of the structure of the surface phase (for example, the degree of order or type of polymorphic modifications), and in the change of its chemical composition (for example, absorption of admixtures, incompatible with the bulk phase structure). If several phases jointly form in the system, SNAPs and not crystal volume parts are in local equilibrium. The relative stability of such systems is accounted for by the principle of continuity of phase formation on coexisting mineral surfaces (Tauson, 2009); according to this principle, SNAPs on various volume phases are able to adapt to each other with the change of physical-chemical growth conditions. This might possibly explain why parageneses retain phases with higher and lower solubility. Heavy metals are transported in hydrothermal fluids in the form of complex compounds. On the surface of growing crystal, these complexes can either disintegrate or react with the surface substance. Disintegrating substance will chaotically settle out on the surface of all jointly generated phases. Nevertheless, if the complex reacts with the surface, it becomes possible to select components through the formation of SNAP, having common structural and chemical elements, both with the matrix, and the given complex. Only a specific complex is able to "extend" SNAPs to a certain critical size, what is an elementary microscopic crystal growth process in such a complex association.

With the increase of SNAP layer thickness, there comes a moment, when the diffusion connection between layer segments adjacent to matrix surface and oversaturated solution is lost; this is followed by transformation of a layer part - coherent or semi-coherent conversion into a matrix crystal structure. During the process, structurally incompatible admixtures are isolated in the form of nano-and microinclusions on defects, pores and other imperfections of the transition zone. SNAP has additional opportunities for accommodation of incompatible elements, therefore, the admixture partially remains in its composition, but its "excessive" part goes from the boundary layer to the surface, forming its own phases. If concentration is related only to the surface layer of SNAP, the content of precious metals increases, but they usually do not reach values, which are sufficient for reliable determination of their chemical forms by XPS method. We managed to obtain such data for Pt and Pd in magnetite crystals (Fig. 3) synthesized in the presence of small additives of chromium, which acted as an indicator of SNAP composition. Forms of Cr(III) confirm its oxyhydroxide nature. Thus, contrary to the generally accepted opinion on the reduction of noble metals on mineral surfaces to a neutral state (Jean, Bancroft, 1995), hydrothermal growth systems demonstrate presence of two forms of each of the elements of Pt and Pd in magnetite – Me(0) and Me(II). This shows that there is not only reductive adsorption as at low, close to normal conditions of P, T -parameters, but also the uptake of these elements by SNAP in chemically bound form. In respect of magnetite, one important fact should be noticed. Adding Mn to the system and causing crystallization of solid solutions (Fe, Mn) [Fe_2O_4], may prevent SNAP formation, up to its disappearance from the surface. This is accounted for by the enrichment of surface with manganese confirmed by the layer-by-layer analysis by LA-ICP-MS method (Tauson et al., 2016). That is, the surface does not contain enough iron to form Fe-oxyhydroxide (similar to hydromagnetite) surface phase.

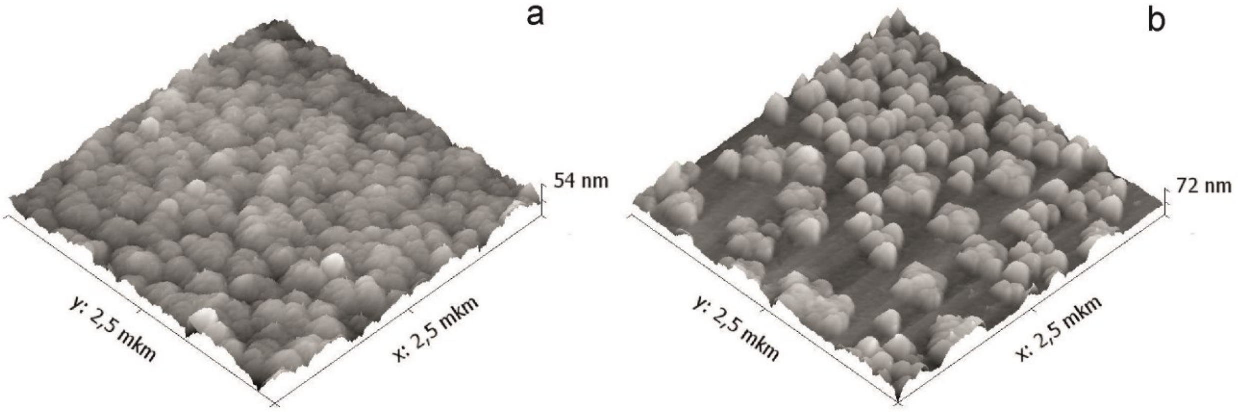

Figure 1. AFM images of galena crystals surface from the experiments with 5 (a) and 10% (b) solution of the mineralizer NH_4Cl

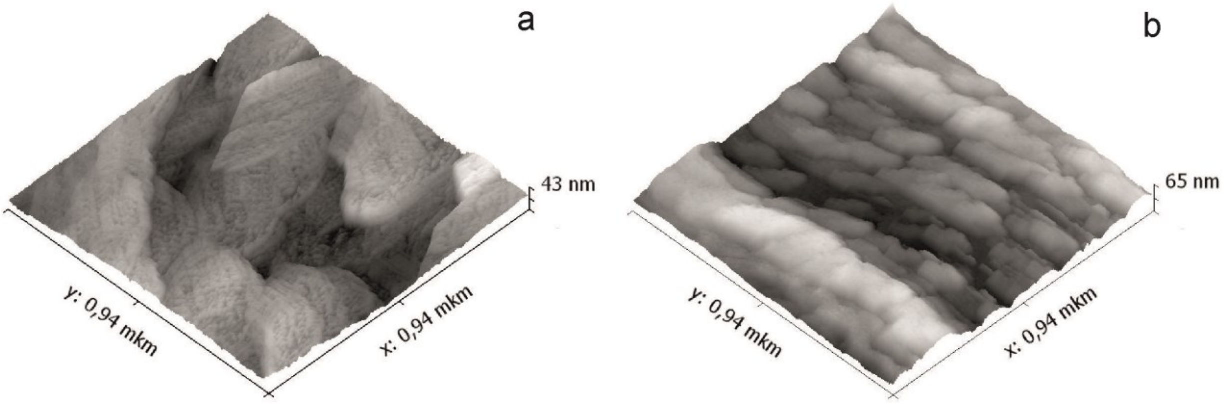

Figure 2. STM images of the surface of magnetite crystals obtained in 5 (a) and 10% (b) solution of the mineralizer

Table 2. Characteristics of the surface of galena and magnetite crystals obtained in solutions with varying concentrations of the mineralizer

	h_{max}, nm	h_{av}, nm	Ra, nm	Rms, nm	S_{tot}/S_{top}
Gn(a)	54.0	29.6	4.5	4.7	1.1
Gn(b)	72.0	36.8	9.5	10.8	1.1
Mt(a)	43.0	21.6	5.0	6.2	1.2
Mt(b)	65.0	34.0	10.0	12.0	1.2

h_{max}, h_{av} – maximum and average height at surface; Ra, Rms – average and root-mean-square surface roughness; S_{tot}/S_{top} – ratio of the total surface to the topographic one.

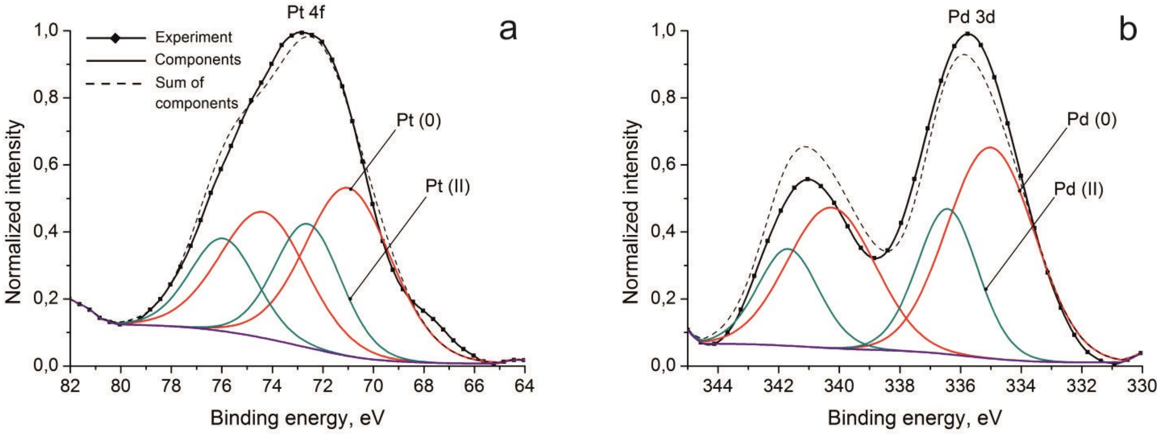

Figure 3. X-ray photoelectronic spectra of Pt 4f and Pd 3d of magnetite crystals. There are registered two valence forms of platinum and palladium – Me(0) and Me(II).

Conclusion. SNAP development is highly dependent on physical-chemical conditions and chemical composition of the medium, which presumes typomorphism and typochemistry of mineral surfaces.

The study is supported by RFBR grants Nos. 15-05-05767, 15-05-00612.

References:

1. Tauson V.L. The principle of continuity of phase formation at mineral surfaces // Doklady Earth Sci. 2009. V. 425A. No. 3. P. 471-475.
2. Tauson V.L., Lipko S.V., Smagunov N.V., Arsent'ev K.Yu., Loginov B.A. Influence of surface nanophases on the processes of crystal formation in multiphase mineral systems // Doklady Earth Sci.. 2014. V. 455. Part 1. P. 317-322.
3. Tauson V.L., Babkin D.N., Pastushkova T.M., Smagunov N.V., Lipko S.V., Voronova I.Yu., Men'shikov V.I., Bryanskii N.V., Arsent'ev K.Yu. Dual distribution coefficients of trace elements in the system mineral-hydrothermal solution. III. Precious metals (Au and Pd) in magnetite and manganmagnetite // Geochem. Internat. 2016. V. 54. No. 2. P. 149-166.
4. Jean G.E.,Bancroft G.M. An XPS and SEM study of gold deposition at low temperatures on sulphide mineral surfaces: Concentration of gold by adsorption/reduction // Geochim. Cosmochim. Acta. 1985. V. 49. P. 979-987.
5. Tauson V.L., Parkhomenko I.Yu., Babkin D.N., Men'shikov V.I., Lustenberg E.E. Cadmium and mercury uptake by galena crystals under hydrothermal growth: A spectroscopic and element thermo-release atomic absorption study // Eur. J. Mineral. 2005. V.17. № 4. P. 599-610.

Rass I.T.[1], Shmulovich K.I.[2]. Trace-element partitioning between apatite and phosphate melt at 0.5 GPa and 900°C.

[1] Institute of Geology of Ore Deposits, Petrography, Mineralogy, and Geochemistry, RAS, Moscow, [2] Institute of Experimental Mineralogy RAS, Chernogolovka Moscow district (rass@igem.ru)

Abstract. Experiments were conducted at 5 kbar, 900°C, and a duration of 9 days using an internally heated pressure vessel. Starting mixtures consisted of CaO, $NaPO_3$, $CaCO_3$, NaF, and nepheline and had variable proportions of phosphate, carbonate, silicate, and fluoride. Oxalic acid, water, and a mixture of trace element oxides (La_2O_3+Sm_2O_3+Yb_2O_3+Y_2O_3+ZrO_2+TiO_2+Nb_2O_5) were added to the starting materials. In two experiments with nepheline-absent starting mixtures, numerous grains with the composition $CaNa_2PO_4F$ were observed in quenched sodium phosphate melt. This phase is similar in composition to the mineral nacaphite from the nepheline syenite of the Khibina massif. The partition coefficients of REE between apatite and melt appeared to be an order of magnitude higher than those reported in three previous publications on the carbonatite system. Compared with apatite–silicate melt partitioning, the REE partition coefficients between apatite and various melts produced in nepheline-bearing mixtures appeared to be 1.5–4 times higher, and the partition coefficients of Ti, Zr, and Nb are higher by 1-2 orders of magnitude.

Keywords: apatite, trace elements, phosphate melt, experiment, partition coefficient

Apatite, a widespread carbonatite mineral, contains REE in concentrations up to a few percent in the form of an isomorphic admixture. Recent experiments aimed at evaluating the distribution coefficients of trace elements between immiscible silicate magma and magmas of other composition (Veksler et al., 2012) have proved that these elements are preferably concentrated in the silicate liquid compared to the carbonate one and also that these elements can be concentrated in fluoride and phosphate (but not carbonate) melts as compared to the silicate ones. Experimental data on the distribution of REE in the course of partial melting in the peridotite-carbonate-phosphate system have discovered immiscibility between the silicate and phosphate-bearing carbonatite melts at high pressures (20-30 kbar) and temperatures 950-1000°C (Ryabchikov et al., 1993) and concentration of REE and Ti(?) in the latter.

Geology of the Kovdor phoscorites – magmatic rocks, genetically associated with carbonatites (Krasnova et al., 2004], data on pyrochlore zoning in the Sokli phoscorite-carbonatite complex (Lee et al., 2006) allow us to suppose an existence of liquid immiscibility between the phosphate-magnetite and carbonatite liquids at lower temperatures, then the experimentally known one of immiscibility between silicate and carbonatite magmas, likely slightly above the solidus temperature of carbonatite magma. A seeming immiscibility between phosphate and carbonatite liquids was first detected in melt inclusions (Andreeva, Kovalenko, 2003) in apatite from the Mushugai-Khuduc carbonatite massif, within the likely temperature range of $500 < T < 900^{o}C$.

In view of the hypothetic existence of phosphate-rich magma in the course of evolution of carbonatite melt after its separation from silicate magma (according to extensive experimental data on 1100–900°C and 1–2 kbar), we have conducted an experimental study in a model phosphate–carbonate system with volatiles. Previously experiments aimed at evaluation of apatite–melt distribution coefficients were carried out only with three carbonatite melts (Ryabchikov et al., 1993; Klemme, Dalpe, 2003; Hammouda et al., 2010) and two silicate ones (Watson, Green, 1981; Prowatke, Klemme, 2006). Our research was focused on determining the apatite–phosphate melt distribution coefficient.

Table 1. Starting materials

No.	CaO mol.%	$CaCO_3$ mol.%	$NaPO_3$ mol.%	NaF mol.%	$NaAlSiO_4$ mol.%	H_2O mg	$H_2C_2O_4$ mg
2	35.67	0	35.62	28.73	0	4.8	2.8
3	27.82	0	55.44	16.70	0	4.5	0.9
4	0	36.92	25.94	37.22	0	4.7	1.8
5	0	35.86	35.87	28.91	0	5.0	1.9
6	0	27.67	55.32	16.70	0	4.8	2.3
7	0	26.30	26.35	26.49	21.07	5.4	2.2
8	0	22.47	45.26	13.45	18.13	5.1	2.1

Experiments were conducted at 5 kbar, 900°C, and a duration of 9 days using an internally heated pressure vessel. Platinum capsules 20 × 3 × 0.1 mm were filled with starting materials with various proportions of CaO, phosphate, carbonate, silicate, fluoride, and nepheline (Table 1), oxalic acid and H_2O. In each capsule, 3–4 mg of powdered and roasted (in a muffle at 800°C) mixture of Ti, Zr, Nb, Y, La, Sm, and Yb oxides were added.

The experimental products from capsules 2–6 with nepheline-free starting materials are aggregates of quenched melt and apatite crystals (**Figs. 1a, b**). The compositions of the quenched melts were analyzed by EMPA with a defocused beam (mostly 30 µm in diameter), Table 2. In runs 4 and 5 the quenched Na phosphate melt contained numerous irregularly shaped domains or numerous crystals of the composition $CaNa_2PO_4F$, which were identical to nacaphite in nepheline syenite from the Khibina Massif (Khomyakov et al., 1981). The phase(?) was analyzed (see crosses in pale gray regions) in 12 domains in capsule 4 and 15 in capsule 5; all of them show a reasonably consistent stoichiometry. The Ap/ sodic phosphate melt distribution coefficients of trace elements, Na, and F were calculated for each run by dividing the average concentrations in the apatite (5–9 spot analyses) into the average concentrations in the melts (25 to 48 EMPA analyses by a defocused beam). The values are given in **Fig. 2** in comparison with the Ap/carbonatite melt distribution coefficients from the aforementioned publications. The REE distribution coefficients between apatite and phosphate melt occurred to be at least one order of magnitude smaller than the values published in papers on the carbonatite system. The Ti, Zr, and Nb distribution coefficients were determined to be higher than the coefficients for apatite/carbonatite melt (Klemme, Dalpe, 2003) and practically exactly equal to those in (Hammouda et al., 2010).

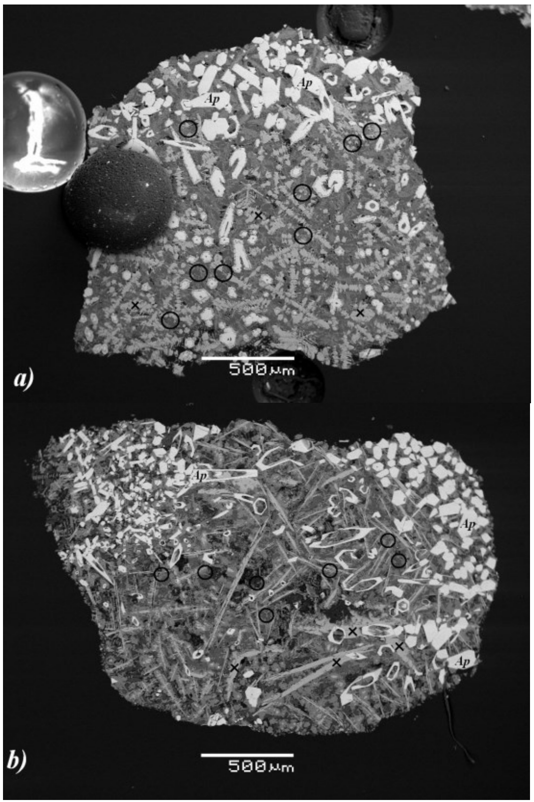

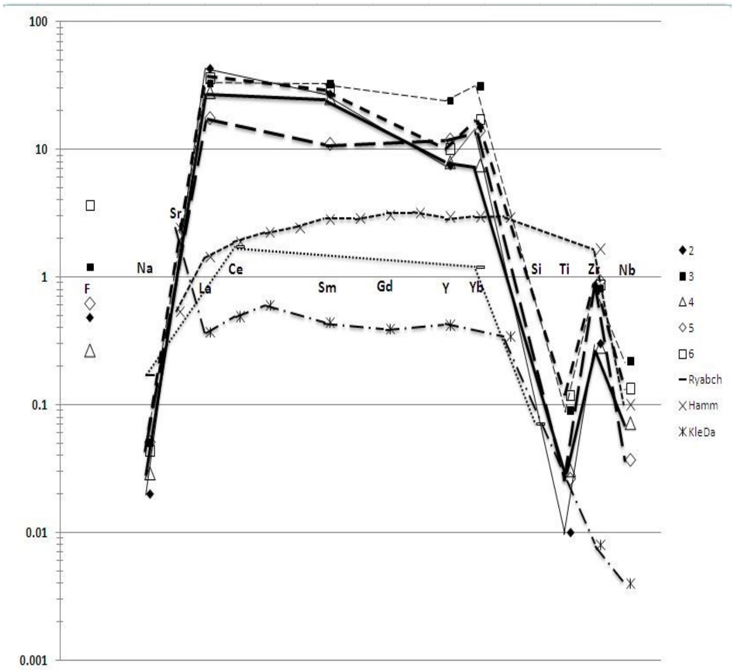

Fig. 1. BSE images of quenched samples: white—apatite in quenched melt, circles—areas analyzed by a defocused beam, and crosses - the pale gray phases(?)—anhydrous F-bearing Na and Ca phosphates (runs 4 and 5 in Figs. 1a and 1b, respectively).

Fig. 2. Ap/sodic phosphate melt distribution coefficients of trace elements, F, and Na in runs 2 and 3 (thin lines) and 4–6 (heavy lines connecting corresponding open symbols 4–6 in the legend) and Ap/carbonatite melt ones from (Ryabchikov et al., 1993; Hammouda et al., 2010; Klemme, Dalpe, 2003)

.

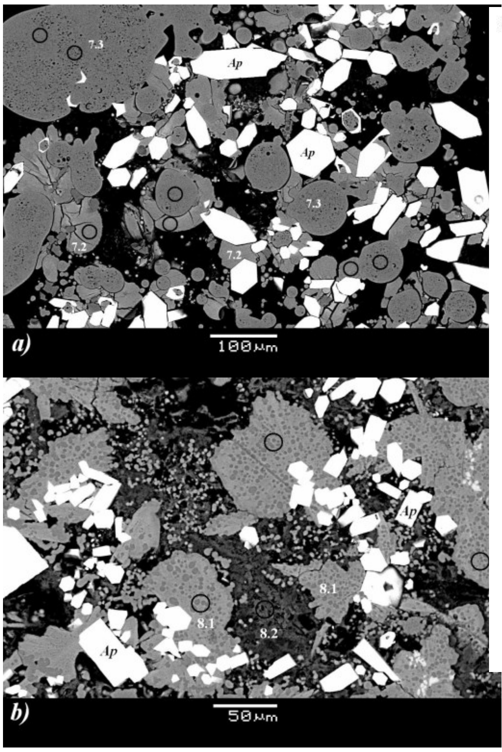

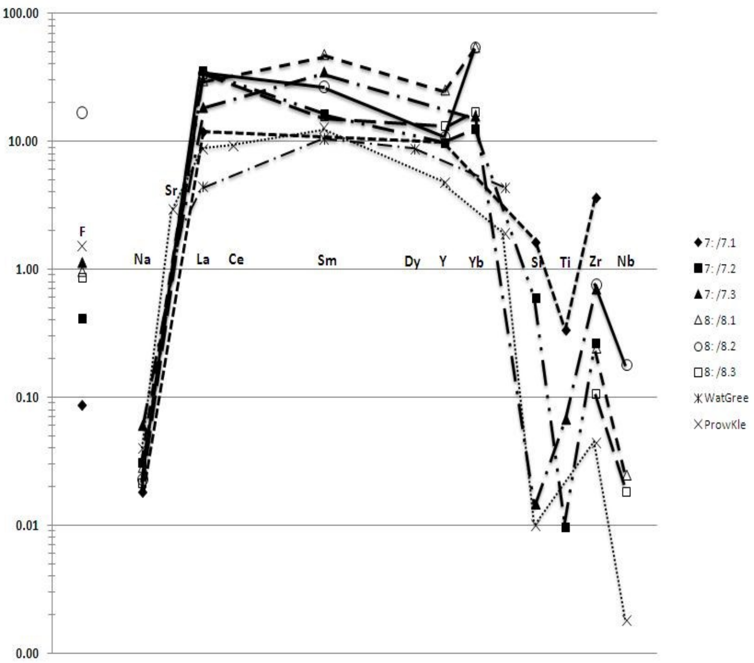

Fig. 3. BSE images of quenched samples: white—apatite, circles—areas analyzed by a defocused beam of different melts(table 2): a) 7.2 and 7.3 in runs 7;b) 8.1 and 8.2 in runs 8.

Fig. 4. Ap/ different melts distribution coefficients of trace elements, F, and Na in runs 7, 8 (heavy lines connecting corresponding solid and open symbols in the legend, respectively) and Ap/silicate melt distribution coefficients from (Watson, Green, 1981; Prowatke, Klemme, 2006).

Table 2. Experimentally received apatite and melt compositions, wt.%

No*	CaO	Na_2O	P_2O_5	F	TiO_2	Nb_2O_5	ZrO_2	Y_2O_3	Yb_2O_3	La_2O_3	Sm_2O_3	SiO_2	Al_2O_3	K_2O	Total-(F=2O)
	the composition of the melt														
2(7)	53,90	0,96	42,29	4,46	0,00	0,00	0,14	0,19	0,32	0,41	0,32				101,13
3(7)	52,54	1,72	42,00	5,07	0,02	0,04	0,28	0,21	0,44	0,49	0,41				98,23
4(9)	53,95	1,15	40,44	4,25	0,01	0,03	0,15	0,08	0,20	0,23	0,21				98,93
5(7)	52,45	1,64	39,55	4,40	0,01	0,01	0,25	0,16	0,29	0,25	0,18				97,34
6(5)	53,46	1,40	41,83	5,40	0,02	0,02	0,25	0,20	0,34	0,36	0,30				101,31
7(6)	53,68	0,90	41,16	3,80	0,01	0,00	0,14	0,19	0,37	0,35	0,33	0,60	0,34	0,14	100,42
8(3)	53,10	0,59	41,24	3,86	0,00	0,01	0,09	0,25	0,54	0,59	0,47	0,00	0,00	0,02	99,14
	the composition of the melt														
2(33)	3,16	41,15	50,72	9,21	0,58	0,48	0,48	0,03	0,02	0,01	0,01				101,98
3(25)	3,42	34,48	54,02	4,26	0,22	0,18	0,35	0,01	0,01	0,02	0,01				95,19
4(36)	6,26	40,21	13,52	16,08	0,44	0,38	0,54	0,01	0,03	0,01	0,01				70,71
5(48)	2,10	32,28	21,10	7,15	0,38	0,27	0,27	0,01	0,02	0,014	0,02				60,61
6(25)	1,75	32,12	45,19	1,49	0,17	0,15	0,29	0,02	0,02	0,01	0,01				80,59
7-1(4)	0,98	49,67	3,49	43,84	0,03	0,03	0,04	0,02	0,00	0,03	0,00	0,37	21,61	0,38	102,03
7-2(15)	3,71	29,6	36,87	9,31	1,05	0,32	0,54	0,02	0,03	0,01	0,02	1,00	13,10	2,07	93,73
7-3(16)	0,51	14,89	5,46	3,36	0,15	0,11	0,20	0,00	0,02	0,02	0,01	40,65	22,00	4,14	90,11
8-1(16)	2,05	20,78	24,33	4,02	0,48	0,23	0,37	0,01	0,01	0,02	0,01	27,32	15,58	2,42	95,94
8-2(13)	0,67	26,15	35,76	0,23	0,01	0,03	0,12	0,02	0,01	0,02	0,02	4,89	3,49	1,11	72,43
8-3(9)	5,81	27,82	37,33	4,47	0,69	0,31	0,84	0,02	0,03	0,02	0,03	6,59	12,16	0,62	94,87

Analists: V. Scherbakov (MSU), E. Kovalchuk (IGEM RAS). *In brackets number of analyses.

Products from capsules 7 and 8, whose starting materials contained nepheline, contain apatite crystals, glasses, and quenched melts (**Figs. 3a, b**) of various composition . The quenched melts were examined with a defocused beam (mostly 30 µm in diameter). The Ap/ different melt distribution coefficients of trace elements, Na, and F in capsuls 7, 8 were calculated for each run by dividing the average concentrations in the apatite (5–9 spot analyses) into the average concentrations in the melts (13 to 18 EMPA analyses). The values are given in **Fig. 4** in comparison with the Ap/silicate melt distribution coefficients from (Watson, Green, 1981; Prowatke, Klemme, 2006). The REE, Ti, Zr, Nb distribution coefficients between apatite and various melts from nepheline-bearing starting materials also occurred to be higher than those from the aforementioned publications.

Acknowledgments. Our thanks to O.G. Safonov, A.V. Girnis, L.S. Moiseeva, D.B. Petrenko for their help.

References:

1. Andreeva I.A., Kovalenko V.I. Magma compositions and genesis of the rocks of the Mushugai-Khuduk carbonatite-bearing alkaline complex (southern Mongolia): evidence from melt inclusions. Per. Mineral 2003, 72, special issue.
2. Hammouda T., Chantel J., Devidal J-L. Apatite solubility in carbonatitic liquids and trace element partitioning between apatite and carbonatite at high pressure. Geoch Cosmoch Acta 2010, 74: 7220-7235.
3. Khomyakov A.P., Kazakova M.E., Pushcharovskiy D.Yu. Nacaphite (Na2CaPO4F) – a new mineral. International Geology Review, 1981, 23: 739-740.
4. Klemme S., Dalpe C. Trace-element partitioning between apatite and carbonatite melt. Amer. Mineral. 2003, 88: 639-646.
5. Krasnova N.I., Balaganskaya E.G., Garcia D. Kovdor – classic phoscorites and carbonatites. In: Zaitsev A.N., Wall F. (eds) Phoscorites and carbonatites from mantle to mine: the key example of the Kola alkaline province. Min. Soc. of Great Britain & Ireland, London, 2004: 99-132.
6. Lee M.J., Lee J.I., Garcia D., Moutte J., Williams C.T., Wall F., Kim Y. Pyrochlore chemistry from the Sokli phoscorite-carbonatite complex, Finland: implications for the genesis of phoscorite and carbonatite association. Geochem. J., 2006, 40: 1-13.
7. Prowatke S., Klemme S. Trace element partitioning between apatite and silicate melts. Geoch Cosmoch Acta, 2006, 70: 4513-4527.
8. Watson E.B., Green T.H. Apatite/liquid partition coefficients for the rare earth elements and strontium. Earth Planetary Science Letters, 1981, 56: 405-421.
9. Ryabchikov I.D., Orlova G.P., Senin V.G., Trubkin N.V. Partitioning of rare earth elements between phosphate-rich carbonatite melts and mantle peridotites. Mineral Petrol., 1993, 49: 1-12.
10. Veksler I.V., Dorfman A.M., Dulski P., Kamenetsky V.S., Danyushevsky L.V., Jeffries T., Dingwell D.B. Partitioning of elements between silicate melt and immiscible fluoride, chloride, carbonate, phosphate and sulfate melts, with implications to the origin of natrocarbonatite. Geoch Cosmoch Acta, 2012, 79: 20-40.

Lukanin O.A. The behavior of chlorine during crystallization-induced degassing of granitic magmas at various depths

V.I.Vernadsky Institute of Geochemistry and Analytical Chemistry RAS, Moscow (lukanin@geokhi.ru)

Abstract. The main factors controlling the behavior of chlorine during crystallization-induced degassing of granitic magmas, such as the initial contents of Cl and H_2O in melts ($C^{o}_{Cl}{}^{m}$, $C^{o}_{H2O}{}^{m}$), pressure, and the degree of system openness are considered basing on the results of numerical modeling. At high pressures (>1.6 kbar), isobaric crystallization is accompanied by a decrease in the concentrations of Cl in the melt ($C_{Cl}{}^{m}$) and fluid phase ($C_{Cl}{}^{fl}$). A decrease in pressure in the range of 1.62–0.85 kbar results in a cardinal change in the Cl behavior: the trend of $C_{Cl}{}^{m}$ and $C_{Cl}{}^{fl}$ decrease dominating at high pressures changes to the opposite. At low pressures (<0.85 kbar), the enrichment of the residual melts and released fluids in Cl leads at a certain stage of crystallization to the formation of a heterogeneous fluid consisting of two immiscible aqueous chloride phases, a waterdominated aqueous phase and a chloride-rich liquid (brine).

Keywords: chlorine, aqueous chloride fluid, granite melt, rhyolite, magma degassing, aqueous chloride brine, computer model

Introduction. Cl-bearing aqueous fluids play an important role in the extraction of major, ore and rare elements from magmas during their degassing. Numerical simulation of granitic magmas degassing is able to determine the main factors controlling Cl partitioning between a melt and an aqueous chloride fluid forming during magma crystallization at different crustal levels. The calculations were carried out using a computer model of degassing developed on the basis of the analysis of available experimental data for the system granitic melt (rhyolite)–H_2O–Na(K)Cl (Lukanin, 2015, 2016). The model accounts for the empirical dependence of Cl partition coefficient between fluid and melt ($D_{Cl}{}^{fl/m}$) on the Cl content of the melt ($C_{Cl}{}^{m}$) and pressure. It allows the calculation of Cl and H_2O redistribution between melt and fluid during isobaric crystallization of a melt over a pressure range of 4 to 0.5–0.3 kbar at a varying degree of openness of the magmatic system with respect to fluid, which can be retained in the system or removed completely or partly. In addition, the model can be used to determine conditions of the formation of a heterogeneous fluid during magma crystallization (the initial contents of Cl and H_2O in the melt, pressure, and a degree of melt crystallization), which represents two immiscible aqueous chloride solutions: water-rich fluid (aq) and

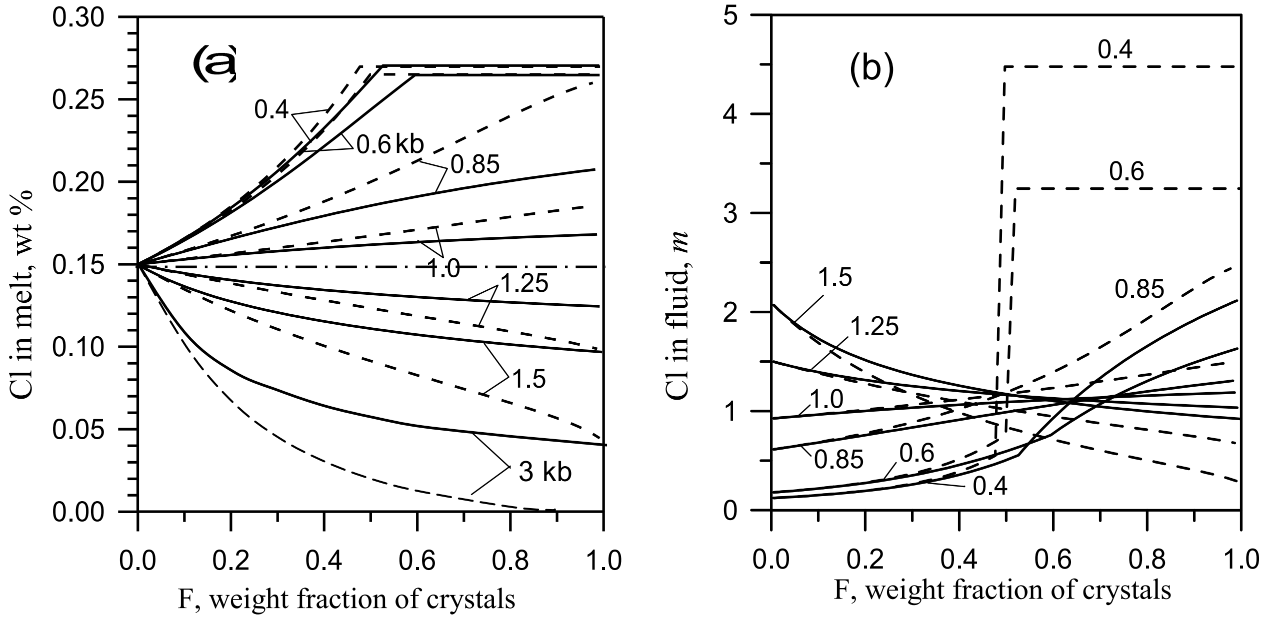

Fig. 1. Influence of pressure on the concentration of Cl in melt (a) and fluid (b) during isobaric crystallization-induced degassing in the pressure range of 0.4–3 kbar. The diagrams show the degassing of melts with the constant initial Cl content of 0.15 wt %. The initial contents of H_2O in melts (wt %): 1.98 (0.4 kbar), 2.57 (0.6 kbar), 3.21 (0.852 kbar), 3.55 (1 kbar), 4.09 (1.25 kbar), 4.59 (1.5 kbar). Solid lines show trends for a closed system, and dashed lines show trends for fractional degassing in an open system. Numbers at the curves are pressure in kbar.

Cl-rich brine (lq), and calculate variations in the composition and amount of fluid phases during degassing.

Results of modeling. The results of numerical modeling show that a decrease in pressure from 4 to 0.4 kbar leads to a drastic change in the behavior of Cl during crystallization-induced degassing (Fig. 1). There are three pressures ranges, that are characterized by specific features of isobaric crystallization-induced degassing: I—*high pressure range* (P > 1.6 kbar), over which the degassing is accompanied by a decrease in the contents of Cl in melt and fluid with increasing degree of crystallization; II—*moderate pressure range* (0.85 < P < 1.6 kbar), over which C_{Cl}^{m} and C_{Cl}^{fl} may increase, decrease or remain constant during crystallization-induced degassing depending on the Cl/H_2O ratios of the initial melts; III—*low pressure range* (0.3– 0.4< P < 0.85 kbar), which exhibits a trend toward the enrichment of residual melts and fluids in Cl during crystallization-induced degassing of initial melts irrespective of their Cl/H_2O ratios. In addition, this pressure range is characterized by heterogeneity of originally homogeneous fluids, i.e. their separation into aq and lq at a certain step of crystallization.

The effect of pressure. During isobaric crystallization of a melt undersaturated with respect to the volatile components at given P–T conditions, water, Cl (and other incompatible components) will be accumulated in the residual melt, until the saturation of melt with respect to volatiles of the fluid phase is reached. Since then, each new step of crystallization (ΔF) is accompanied by the release of H_2O and Cl into the fluid phase and the H_2O content of the residual melt remains almost constant, despite minor variations in the content of both major components and volatiles (including Cl) in the melt. However, the amount of H_2O released to the fluid strongly depends on pressure during crystallization of any given portion of the silicate phase (at a crystallization step of ΔF). The higher the pressure, the higher the initial H_2O content of the melt to the beginning of degassing and, consequently, the larger portion of H_2O is released from melt at each new step of crystallization. The amount of Cl released from melt is controlled by the $D_{Cl}^{fl/m}$ value and the fluid (water)/melt mass ratio. Considering the very high values $D_{Cl}^{fl/m}$ at high pressures (>1.62 kbar) and the amount of water released from melt after each new step of crystallization, Cl will be preferentially partitioned into the fluid phase. At the same time, the amount of Cl transferred from the melt into the fluid is much higher than excess Cl that should remain in melt after a given step of crystallization if Cl would behave as an incompatible element and the fluid phase would be absent at all in the system or $D_{Cl}^{fl/m}$ would be equal to zero. As a result, the Cl content of melt decreases.

A decrease in P results in a decrease in $D_{Cl}^{fl/m}$ and $C^{o}_{H_2O}{}^{m}$ and, correspondingly, in the mass of H_2O released to the fluid after each step of crystallization. A decrease in C_{Cl}^{m} at a given P also results in a decrease in $D_{Cl}^{fl/m}$. Therefore, the degree of Cl extraction from the residual melt during isobaric crystallization will decrease with decreasing pressure and $C^{o}_{Cl}{}^{m}$. For melts with $C^{o}_{Cl}{}^{m}$ = const, the concentrations of Cl in melt and fluid remain unchanged as P decreases to a certain P_i value. This implies that the amounts of Cl and H_2O released after crystallization of a portion of melt over the interval of ΔF will be completely transferred to the fluid phase.

A further decrease in P and, correspondingly, in and the mass of H_2O released from the melt causes only part, not all, of excess Cl to transfer from the residual melt to the fluid. This results in an increase in both C_{Cl}^{m} and C_{Cl}^{fl}. It should be noted that C_{Cl}^{m} increases during crystallization-induced degassing at $D_{Cl}^{fl/m}$ much higher than one. This apparent contradiction can be explained by the presence of crystalline phases, in addition to melt and fluid, in the system. Therefore, the C_{Cl}^{m} values will be controlled by the combined (bulk) Cl partition coefficient between the melt and the remaining phases ($D_{Cl}^{m/\#}$). For simplicity, all crystallizing silicate phases are regarded in a first approximation as a single solid phase (s). Then:

$$D_{Cl}^{m/\#} = C_{Cl}^{m}/(C_{Cl}^{fl}\, x^{fl} + C_{Cl}^{s}\, x^{s}), \qquad (1)$$

where C_{Cl}^{s} is the concentration of Cl in the solid phase, x^{fl} and x^{s} are the weight fractions of the fluid and solid phase, respectively, (if the concentrations of Cl in wt % are used for the calculation of $D_{Cl}^{fl/m}$) in the mixture fluid + solid phase. If $C_{Cl}^{s} = 0$, i.e., Cl behaves as a completely incompatible element during crystallization, then (1) can be written as:

$$D_{Cl}^{m/\#} = 1/\, D_{Cl}^{fl/m}\, x^{fl}\ . \qquad (2)$$

The $D_{Cl}^{fl/m}$ value distinctly decreases with decreasing P and C_{Cl}^{m}; however, it remains higher than one at pressures from 4 up to 0.4 kbar for melts with $C_{Cl}^{m} \geq 0.01$ wt %. The weight fraction of the fluid phase depends almost only on the mass of water released during crystallization of a melt, therefore, it also decreases with decreasing P. As a result, $D_{Cl}^{m/\#}$ increases progressively with decreasing P ($C^{o}{}_{Cl}^{m}$ = const) until it approaches the value higher than one at a certain P_i, which causes an increase in C_{Cl}^{m} during isobaric crystallization-induced degassing. The inversion pressure P_i corresponds to the condition when $D_{Cl}^{m/\#} = 1$. Note that if $C_{Cl}^{s} > 0$, then P_i decreases slightly with increasing C_{Cl}^{s} (for melts with $C^{o}{}_{Cl}^{m}$ = const). Similarly, for the combined (bulk) Cl partition coefficient between the fluid and the remaining phases in the system (melt + crystals), $D_{Cl}^{fl/\#}$, at $C_{Cl}^{s} = 0$, the following equation is valid:

$$D_{Cl}^{fl/\#} = D_{Cl}^{fl/m}/x^{m}\,, \qquad (3)$$

where x^{m} is the weight fraction of the melt in the mixture melt + solid phase. Since $x^{m} \leq 1$, then $D_{Cl}^{fl/\#} \geq D_{Cl}^{fl/m}$ and, correspondingly, $D_{Cl}^{fl/\#}$ always increases during crystallization with decreasing x^{m}. Therefore, at $D_{Cl}^{fl/m} > 1$, an increase in C_{Cl}^{m} during crystallization at low pressures will be accompanied by an increase in the concentration of Cl in the fluid.

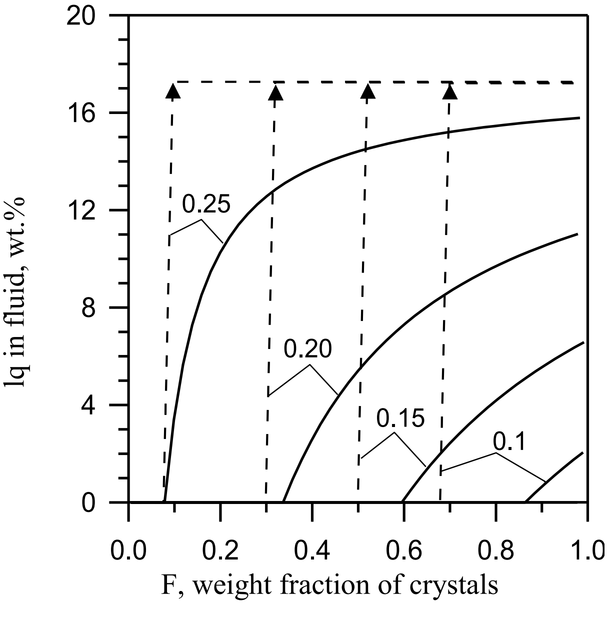

Fig. 2. The amount of aqueous chloride brine (lq) that formed in the fluid during crystallization-induced degassing at 0.6 kbar. It is assumed that Cl is present in lq and aq as NaCl. The concentration of NaCl in lq is taken to be equal to 72 wt %, according to the data of Bodnar et al. (1985) for the H_2O–NaCl system at 0.6 kbar and 800°C. Numbers at the curves are the initial Cl contents of the melt (in wt %). Solid lines show trends for a closed system, and dashed lines show trends for fractional degassing in an open system. Dashed lines with arrows show the degree of crystallization under open-system conditions, leading to the formation of a heterogeneous fluid having a constant aq/lq ratio and, correspondingly, constant composition.

The results of numerical modeling show that for melts saturated in a fluid phase aq or aq + lq, the inversion of Cl behavior depending on $C^{o}{}_{Cl}^{m}$ occurs over the range of pressures from 1.62 kbar (for melts strongly depleted in Cl with $C^{o}{}_{Cl}^{m} < 0.001$ wt %) to 0.85 kbar (for melts strongly enriched in Cl with $C^{o}{}_{Cl}^{m} = 0.26$ wt %). At pressures below 0.85 kbar, the concentration of Cl in the released fluid increase to such a extent that the fluid separates into two phases, aq and lq. Further crystallization occurs with no change in composition of all coexisting phases (m + aq + lq) while their proportions change. In a closed system, the amount of melt decreases with increasing lq/aq. In an open system, the aq/lq ratio of the fluid remains unchanged with decreasing amount of melt. The important factors controlling the formation of a heterogeneous fluid at the earlier stages of crystallization are a decrease in total pressure, an increase in Cl/H_2O of the initial melt and an increase in the degree of system openness.

Heterogeneous fluid composition. The lq/aq ratio in a heterogeneous fluid at given *P* and *T* depends on the initial volatile contents of melts and the degree of melt crystallization. Figure 2 shows the effect of the degree of crystallization and $C^o_{Cl}{}^m$ on the amount of an aqueous chloride liquid (brine, lq) in the fluid released during crystallization-induced degassing at 0.6 kbar. In a *closed system*, the amount of lq formed during the final stages (F ≥ 0.87) of the degassing of melts with $C^o_{Cl}{}^m = 0.1$ wt % does not exceed 2 wt %. At the same time, the phase lq appears during the early stages of degassing of melts with $C^o_{Cl}{}^m = 0.2$ wt % at F ≥ 0.34 and reaches a maximum of 11 wt % at the final stages of crystallization. At this pressure, the maximum amount of lq (17.3 wt %) is observed in fluids that are released during the degassing of melts with $C^o_{Cl}{}^m$ corresponding to the m + aq + lq equilibrium (0.265 wt %). A similar content of lq will be observed in heterogeneous fluids formed in an *open system* during the degassing of all melts with initial Cl contents ranging from ~0.05–0.1 to 0.265 wt %.

With the appearance of a heterogeneous fluid and an increase in the lq/aq ratio during degassing under closed-system conditions, an increasing part of Cl removed from the silicate phase will be redistributed to lq.

Conclusions. As opposed to the model system rhyolite–H_2O– Na(K)Cl, crystallization of natural magmas may be accompanied by simultaneous changes in *T, P*, the compositions of residual melts with respect to major components, and the degree of system openness. H_2O- and Cl-bearing minerals as additional crystallizing phases can also be present. Therefore, the inferred boundaries of pressure and initial volatile contents controlling the behavior of Cl during degassing of model melts are expected to move to one or another side and be not so sharp. At the same time, the characteristic features of Cl behavior during crystallization-induced degassing of granite magmas at different depths obtained from numerical experiments must be observed in nature. The same is true for the inversion of the pressure dependence of Cl behavior, when the depletion of fluids and residual melts in Cl with decreasing pressure changes to the accumulation of Cl in the fluid and the formation of aqueous chloride brines at a certain stage of crystallization.

References:

1. Lukanin O.A. (2015) Chlorine partitioning between melt and aqueous chloride fluid during granite magma degassing. Part I. Decompression-induced melt degassing. *Geochemistry International,* **53** (9), 786–810.
2. Lukanin O.A. (2016) Chlorine Partitioning between Melt and Aqueous Chloride Fluid Phase during Granite Magma Degassing. Part II. Crystallization-Induced Degassing of Melts. *Geochemistry International*, **54 (**8), 660–680.